Tunable mid-infrared laser sources for trace-gas analysis

Tunable mid-infrared laser sources for trace-gas analysis

D B Kolker[1,2,3], I V Sherstov[1,2], A A Boyko[1,2,4], B N Nyushkov[1,3], E Y Erushin[1,2,3], N Y Kostyukova[1,2,3], A I Akhmathanov[5], A Y Kiryakova[3] and A V Pavluck[1]

[1] Novosibirsk State University, 1 Pirogova str., Novosibirsk, 630090, Russia
[2] Institute of Laser Physics SB RAS, 15B, Ac. Lavrentyev ave, Novosibirsk, 630090, Russia
[3] Novosibirsk State Technical University, 20 K. Marx ave, Novosibirsk, 630073, Russia
[4] Tomsk State University, 36 Lenin av. Tomsk, 634050, Russia
[5] Ural Federal University, 19 Mira Street, Yekaterinburg, 620002, Russia

Abstract. We demonstrate advanced experimental approaches to photoacoustic gas detection with tunable mid-infrared (mid-IR) laser sources of different types. A gas analyzer for registration of various gas components based on a tunable narrow-linewidth optical parametric oscillator (OPO) was designed and investigated. Using this OPO, the possibility of measuring the trace concentration (~2÷3 ppm) of methane (CH_4) in air was experimentally shown. The gas detection capability was enhanced by introducing injection seeding into the OPO. Another gas analyzer was based on a quantum cascade laser (tunable within the range ~7.6 ÷7.7 μm) and a resonant differential photoacoustic detector. Detection of the ultra-low concentration (~0.3 ppm) of methane in air was achieved (the standard dispersion was (1σ) ≈ (10–11) ppb with an integration time of 10 s). We compare the presented approaches and outline their further development.

1. Introduction

Tunable optical parametric oscillators, as well as quantum-cascade lasers, are currently used as laser sources for remote and local gas analysis. This paper presents experimental gas analytical systems and prototypes of operating devices based on optical parametric oscillators and quantum cascade lasers.

The mid-IR range (2-14 μm) is of great interest for various applications. It contains fundamental vibrational-rotational absorption bands of various gases, which allows remote [1, 2] or local gas analysis of the atmosphere [3, 4] using lasers with appropriate wavelengths. The absorption of water vapour in the atmosphere significantly limits the spectral regions in which laser radiation passes through the open atmosphere. The main transparency windows of the atmosphere are located in the ranges of 3-5 μm and 8-12 μm. In addition to water vapour, atmospheric carbon dioxide, which has strong broad absorption bands centred near 4.3 and 14 μm, also restricts the propagation of laser radiation. In the spectral range of 8-12 μm, tunable CO_2 lasers are traditionally used for various purposes (including atmospheric gas analysis). These lasers emit at various vibrational-rotational transitions in the range of 9.2-10.8 μm [5,6]. Optical parametric oscillators (OPOs) and quantum cascade lasers (QCLs) are widely used in the range of 3-5 μm and 8-12 μm [10]. Currently, gaseous pollutants such as sulfur dioxide (SO_2), nitrogen oxides (NO_x), and hydrocarbons (HC), as well as their reaction products, such as acids and oxidants, are of primary interest. SO_2, NO_x and hydrocarbons are the primary pollutants, while the reaction products are referred to as secondary pollutants. In industrialized countries with high traffic density, air pollution is mainly caused by human activities, that is, anthropogenic sources. In contrast, the contribution of natural sources to air pollution is often

negligible. In Europe, the importance of SO_2 as an air pollutant has been slowly declining since ~ 1970 due to the decline in the sulfur content of fuel oil used for heating. On the contrary, NO_x and HC emissions are increasing. As a result, by the beginning of the XXI century, their concentrations turned out to be about 10 times higher than in the middle of the XX century. This increase is mainly related to cars, as up to 70% of NO_x emissions and ~ 25% of HC emissions are caused by vehicles.

The processes of global warming on Earth are also causing great concern to scientists around the planet. Currently, the background concentration of CO_2 as the main "greenhouse gas" has exceeded 400 ppm. Various international agreements (Kyoto Protocol, Paris Climate Agreement, etc.) call for limiting and reducing carbon dioxide emissions into the atmosphere in the future. For this, new technologies are being developed, the so-called. "Green energy" with renewable energy sources (solar energy, the use of wind energy, tidal power plants, etc.).

2. Optical parametric oscillators

2.1. *Fan-out-PPLN-based pulsed OPO with injection seeding*

OPOs are universal solid-state coherent sources with the possibility of wavelength tuning in the aforenamed spectral range. However, conventional OPOs without special measures for spectral narrowing feature relatively broadband radiation spectra (up to dozens of nanometers) which impede performing high-resolution spectroscopy. Therefore, special methods are applied in OPO design to narrower optical spectra of generated mid-IR radiation. These methods may include, for example, the use of injection-seed lasers [7-15], or the use of a spectral-selective element, such as an etalon, diffractive grating, or a volume Bragg grating, in the OPO cavity [16-19]. Here, we present an original narrow-linewidth pulsed OPO configuration which employs fan-out periodically-poled lithium niobate (fan-out PPLN) and injection seeding laser sources of two different types adapted for the PA sensing of methane. The developed experimental setup is shown in figure 1.

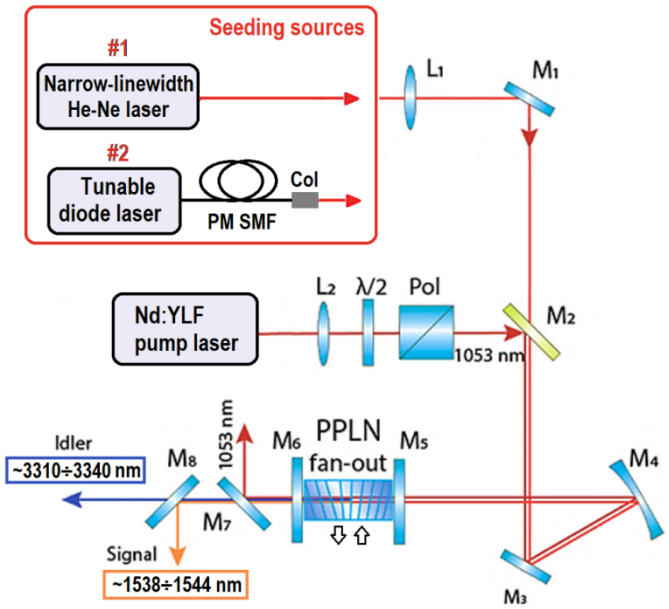

Figure 1. Schematic of the injection-seeded fan-out-PPLN-based OPO developed for PA gas sensing

Two alternative continuous-wave seed lasers were used in our experiments: a fibre-coupled distributed-feedback (DFB) diode laser with a megahertz linewidth at ~1.54 μm and a He-Ne laser

with a kilohertz linewidth at 3.39 μm. The pumping and seeding radiation beams were matched with the OPO cavity by using lenses and dichroic mirrors. When the diode laser was used instead of, the He-Ne laser, the mirrors M_2 and M_5 were replaced accordingly with the seed wavelength. The OPO cavity was designed to be resonant for the signal wave at around 1.54 μm, thereby allowing the idler wave to be obtained at around 3.39 μm which allows for matching with an absorption line of methane. Without injection seeding laser, the tuning range of the idler wave can be in principle as wide as 1778 cm^{-1} (2.5-4.5 μm) [20]. The dichroic mirror M_7 filters out the residual pump radiation from the output beam containing signal and idler waves. In turn, the dichroic mirror M_8 splits the idler and signal waves, thereby allowing the idler wave to be used for PA gas sensing and the signal wave to be used for monitoring the OPO output with a commercial λ-meter (Angstrom IR II WS6). Thus, the developed OPO system can operate alternatively in two modes: with the injection seeding wave coinciding either with the signal wave (the diode seed laser at 1.54 μm) or the idler wave (the He-Ne seed laser at 3.39 μm). Both types of seeding provided spectral narrowing of the OPO system and thus improved the sensitivity of methane detection with a PA method. The options provided by these different types of seeding are the following: the DFB diode laser enables fine wavelength tunability [21], while the He-Ne laser provides stronger spectral narrowing [22] and can in principle ensure excellent wavelength stability of a metrological grade [23].

Figure 4 illustrates spectral narrowing achieved in the OPO upon injection of seeding radiation from the He-Ne laser. This spectral narrowing provides an improved response (higher sensitivity) of photoacoustic detection of the methane as illustrated in figure 2. This figure shows the response of the photoacoustic detector PAD-90 [24] to 3 different events: track 1 is the detector response to room air (background level of methane concentration); track 2 is the response to the test gas mixture N_2+1000 ppm CH_4 when seed laser is off; track 3 is the response to the test gas mixture N_2+1000 ppm CH_4 when seed laser is on. The PAD response is increased by a factor of ~2 when seed laser is used.

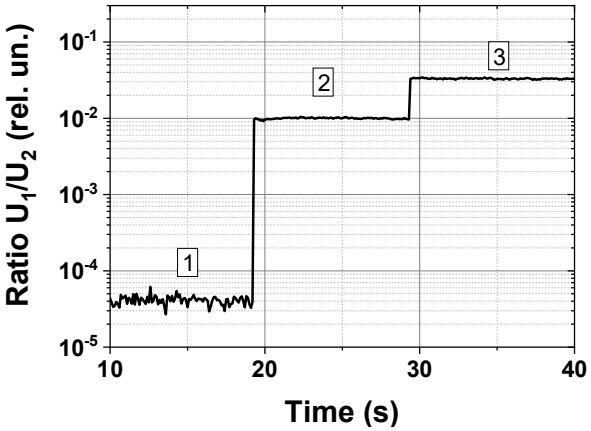

Figure 2. The response of the photoacoustic methane detector employing the developed OPO: track 1 is the detector response to room air (background level of methane concentration); track 2 is the response to the test gas mixture N_2+1000 ppm CH_4 when seed laser is off; track 3 is the response to the test gas mixture N_2+1000 ppm CH_4 when seed laser is on

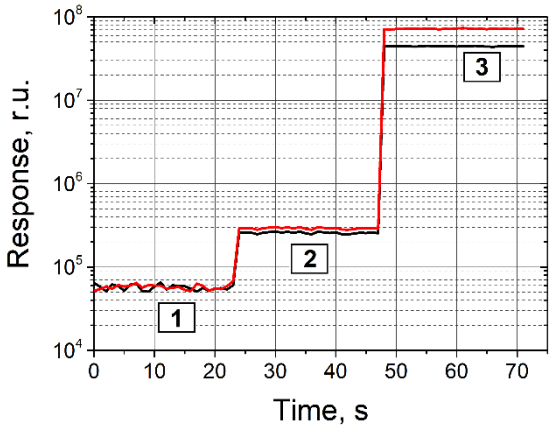

Figure 3. The responses of the photoacoustic methane detector employing the developed OPO under free-running (black trace) and injection-seeded (red trace) conditions: 1 – response to the dry nitrogen, 2 – response to the room air (~1.86 ppm of CH_4), 3 – response to the reference gas mixture (N_2+1000 ppm of CH_4)

We have also explored the possibility to enhance methane detection capabilities of the fan-out-PPLN-based OPO by combining its own wavelength tunability with the tunability of the aforenamed

diode-laser seed source. Such injection seeding at the signal wavelength also ensures spectral narrowing of the OPO radiation and improves the response of the photoacoustic methane detector [21].

Figure 5 illustrates spectral narrowing achieved in the OPO upon injection of tunable seeding radiation from the DFB diode laser. This spectral narrowing along with fine wavelength tuning ensures improved response (higher sensitivity) of photoacoustic detection of the methane as illustrated in figure 3. This figure shows the response of the photoacoustic detector PAD-90 [24] to 3 different events under free-running (black trace) and injection-seeded (red trace) conditions: 1 – response to the dry nitrogen, 2 – response to the room air (~1.86 ppm of CH_4), 3 – response to the reference gas mixture (N_2+1000 ppm of CH_4). The use of the seed laser provides an almost double (~80%) increase in the photoacoustic response.

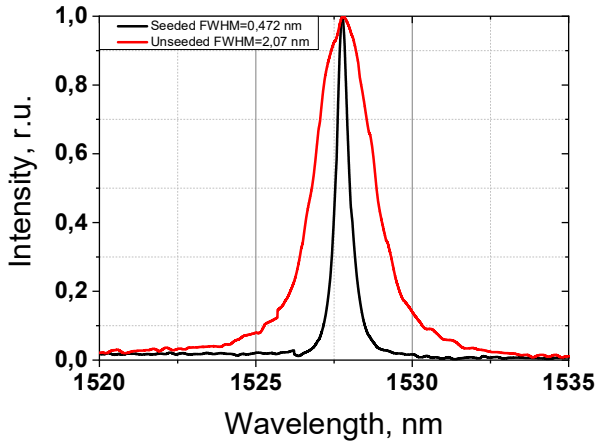

Figure 4. Optical spectra of the OPO signal radiation obtained without (red curve) and with (black curve) seeding radiation from the He-Ne laser

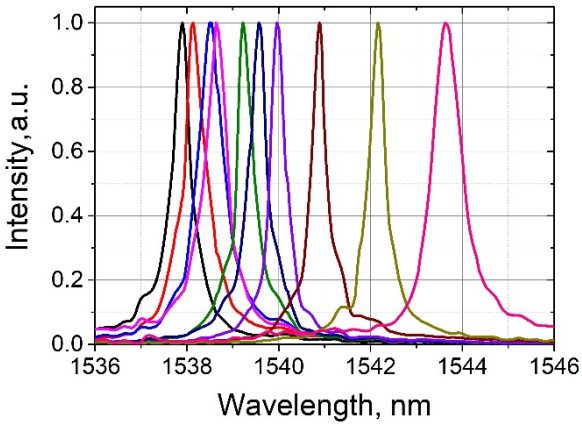

Figure 5. Optical spectra of the OPO signal radiation obtained with tunable seeding radiation from the DFB diode laser

It is worth noting that that the implemented injection seeding provides not only a significant narrowing of the OPO radiation spectrum but also noticeably stabilize its central wavelength [21].

We also anticipate that the above injection seeding technique can be further improved by applying a seed laser source with a much wider wavelength tuning range (like an ultra-widely tunable Er-fiber laser [25]). Useful options might be granted to the OPO also by a pulsed seed source with the arbitrary controllable timing (like that of a hybrid laser demonstrated in [26]). Such improvements will extend the tunability of spectral and temporal characteristics of the pulsed OPO radiation.

2.2. HGS-crystal-based OPO

Figure 6 shows an OPO experimental setup at 4.5-10 μm based on mercury thiogallate crystals. The OPO is pumped by an Nd: YLF laser in the region of 1.053 μm. The pulse repetition rate varied from 0.02 kHz to 4 kHz, and pulse duration was 5-7 ns. The pump radiation passes through the Faraday isolator, the λ/2 plate and, using the M_3 mirror and the M_4 dichroic mirror (passes the signal and idler, reflects the pump), is directed into the OPO cavity, which is formed by the M_1 and M_2 mirrors. The OPO cavity is formed by two flat mirrors: a metal mirror with a reflection coefficient of R = 97% for emission of all three waves (pump, signal, and idler) and a ZnSe input/output mirror with a high transmittance for pump radiation (T = 92% @ 1.053 μm) and idler wave (T = 80% @ 4.2-10.8 μm), and high reflectivity for signal wave emission (R ~ 95% @ 1.17-1.4 μm).

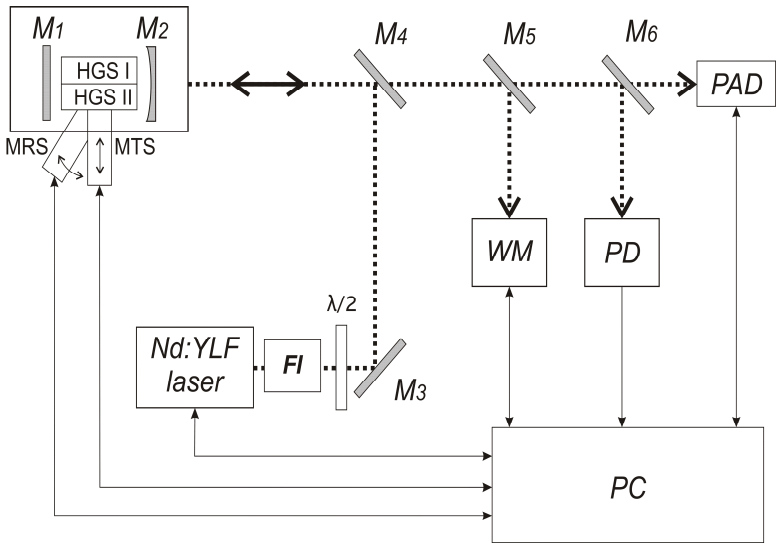

Figure 6. The part (4.5-10.8 μm) of combined OPO based on two $HgGa_2S_4$ crystals [9]

Both HGS crystals (Figure 6) are oriented for the second type of interaction (eo-e), but with different cut angles. The HGS I crystal was cut at an angle θ=60 °, φ=0 °, which corresponds to an idler wavelength of ~ 4.7 μm at normal incidence of pump radiation on the crystal, the HGS II crystal was cut at an angle θ=47 °, φ=0 ° (for an idler wavelength ~ 7.45 μm at normal incidence). The HGS I crystal has the following dimensions: 5x4.5x11 mm, and the HGS II 6x4.3x13.7 mm. To minimize optical losses in the cavity, a single-layer antireflection coating with a centre of 1.2 μm was applied to the ends of both crystals. The tuning of the OPO wavelength was carried out by motorized rotary stage (MRS) rotating the crystals relative to the axis of the OPO resonator, and switching between the crystals was carried out by motorized translation stage (MTS). Part of the OPO radiation on the signal wave is directed to the laser wavelength meter (WM), and the idler wave is directed to the optical-acoustic detector. In this case, a small part (4%) of the idler wave is directed by the M_6 mirror to the reference pyroelectric detector.

Figure 7 shows the OPO performance (idler wave) at ~5.05 μm. The HGS-OPO threshold was ~33 mJ/cm^2. The conversion efficiency of the pump energy into idler wave energy was about 3.1%, the differential efficiency was 4.28%, and the quantum efficiency was 14.86%.

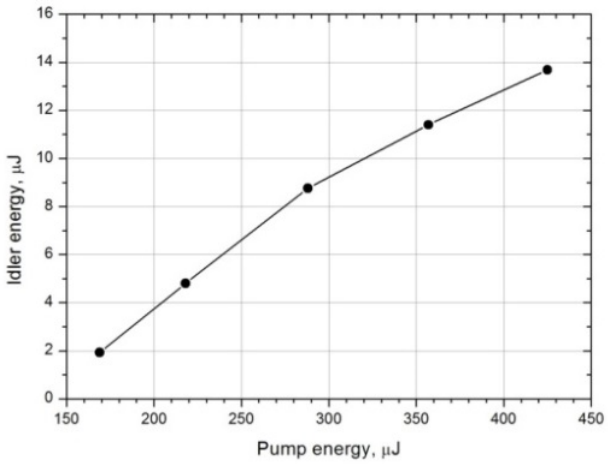

Figure 7. Performance of HGS-OPO at 5.05 μm

3. Quantum cascade lasers

In this work, we used a QD7500CM1 QCL (Thorlabs, Inc.), which is a compact semiconductor laser in the mid-IR range (λ ~ 7.5 ... 7.7 μm). This QCL is a so-called "DFB laser" - a distributed feedback laser that provides single-mode operations.

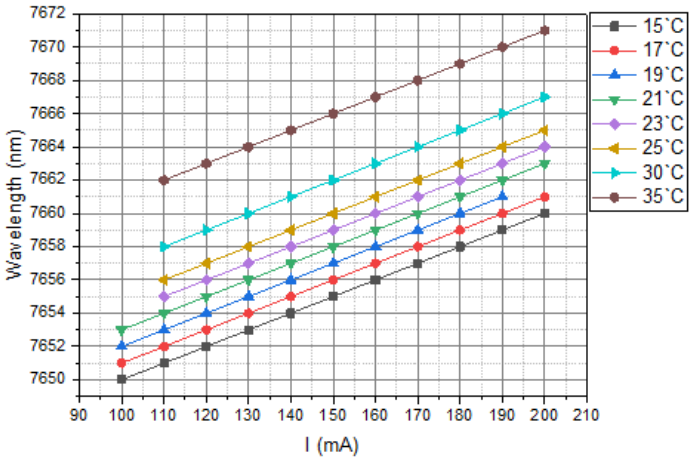

Figure 8. The QCL wavelength tuning curves. Wavelength tuning from injection current and temperature

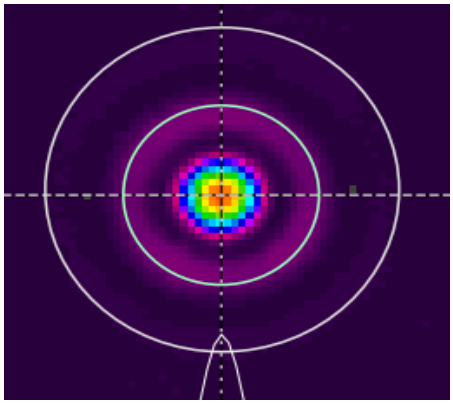

Figure 9. The QCL beam profile (Pirocam IV)

Figure 8 illustrates wavelength tuning of QD7500CM1 QCL (Thorlabs, Inc.) laser as a function of injection current with temperature as a parameter. From figure 8 we are estimating the QCL wavelength tuning range (injection current and temperature) as 7660±10 nm. At least we were obtained ~ 24 mW average powers when the injection current was swiped at the frequency 1700 Hz from 90 to 180 mA. Figure 9 shows the beam profile measured by Pirocam IV.

The photo-acoustic (PA) methane gas analyzer based on a quantum cascade laser (QCL; ~7.7 μm / 1800 Hz / 24 mW), a resonant differential PA detector, and a sealed gas-filled cell was investigated [20]. The measurement of methane concentration below the background value in the air (~0.3 ppm CH_4) is shown, the standard dispersion was (1σ) ≈ (10–11) ppb CH_4 with an integration time of 10 s. Under conditions of temperature instability (or emission wavelength) of QCL when

normalized to a gas-filled cell, the relative measurement error of the CH_4 concentration does not exceed 3% (figure 10).

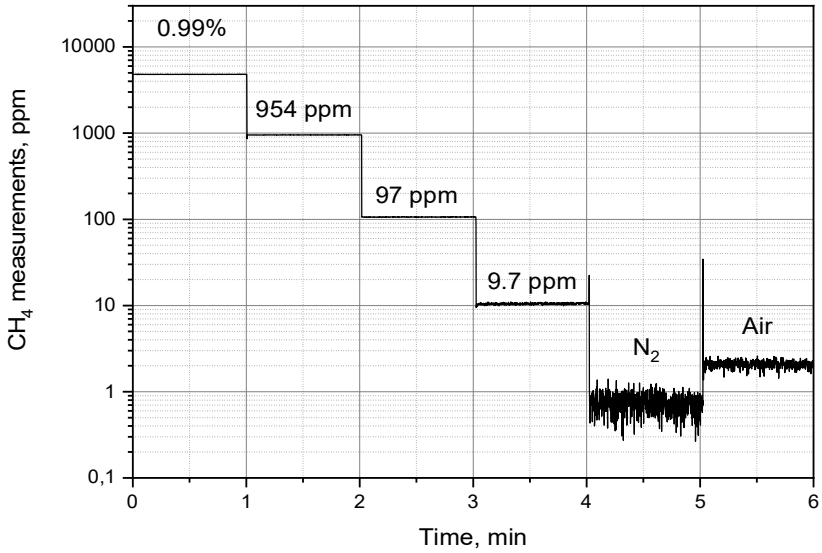

Figure 10. QCL-PAD methane gas analyzer. PAD response from different CH_4 concentrations [28]

4. Summary

Test-bed configurations of gas analyzers for registration of various gas components based on widely tunable OPOs operating in the mid-IR range (at wavelength from ~3 μm to ~10 μm) were demonstrated. The investigation of photoacoustic gas detection through the developed OPO was carried out using the example of methane. The OPO operated at an idler wavelength of ~ 3.3 μm which was used for the methane detection. The possibility of measuring the background concentration of methane in the air (~ 2–3 ppm CH_4) has been experimentally shown. The threshold sensitivity of the studied gas analyzer was (1σ) ~ 49 ppb CH_4.

The demonstrated spectral narrowing (and wavelength stabilization) of the OPO radiation utilizing injection seeding not only improves the response of the OPO-based photoacoustic gas detectors but also enhances the spectroscopic capabilities of OPOs in general. Owing to comparatively high power spectral density and wide tunability, such OPOs may successfully compete with other sources used for precise spectroscopy in mid-IR [28] and far-IR [29] ranges.

Besides that, a unique methane gas analyzer based on a quantum cascade laser at 7.65 μm has been developed as well. The device will be used to map the area for methane leaks and search for oil fields. The sensitivity is at the background level (1.86 ppm). The weight is 3 kg.

A decrease in the average QCL radiation power (~24-12-6 mW) leads to a noticeable deterioration in the threshold sensitivity of the PA gas analyzer. It is recommended to increase the average QCL power level to ~50 mW. The dynamic range of measuring the concentration of methane of the PA gas analyzer in the linear mode was ~4 decades (from 0.3 ppm to 2000-3000 ppm CH_4)

Acknowledgments

This work was partially supported by the Ministry of Science and Higher Education of the Russian Federation (grant FSUS-2020-0036). The Fan-out MgO: PPLN chip was prepared by A.A. and V.S with support from Russian Foundation for Basic Research (grant RFBR-mk-18-29-20077). The CH_4 spectroscopic experiments were funded by RFBR, project number 19-32-60055.

References

[1] Balandin S F and Shishig S A 2006 *Proc. SPIE* 6160 (Tomsk) **Vol. 6160** 61601Z
[2] Ivashenko M V and Sherstov I V 2000 *Quantum Elec.* **30** 747-52
[3] Philippe Repond and Markus W Sigrist, *Appl. Opt.* **35** 4065
[4] Sherstov I V, Kapitanov V A, Ageev B G, Karapuzikov A I and Ponomarev Y N 2004 *Atmospheric Ocean. Opt*. **17** 119-23
[5] Karapuzikov A I, Malov A N and Sherstov I V 2000 *Infrared Phys. Technol.* **41** 77-85
[6] Sherstov I V, Buchkov K V, Vasilyev V A, Karapuzikov A I, Spitsyn V V and Chernikov S B 2005 *Quantum Elec.* **18** 270
[7] Fix A, Schröder T, Wallenstein R, Haub J G, Johnson M J and Orr B J 1993 *J. Opt. Soc. Am. B* **10** 1744
[8] Fink T, Büscher S, Gäbler R, Yu Q, Dax A and Urban W 1996 *Rev. Sci. Instrum.* **67** 4000-04
[9] Petrov V 2015 *Prog. Quantum. Electron.* **42**. 1-106
[10] Elder I, Legge D, Beedell J and Marchington R 2006 *Technical Digest Advanced Solid State Photonics.* paper MB20
[11] Mahnke P, Klingenberg H H, Pix A and Wirth M 2007 *Appl. Phys. B* **89** 1–7
[12] White R T, He Yabai, Orr B J, Kono M and Baldwin K G H 2003 **28** 1248-50
[13] Plusquellic D F, Votava O and Nesbit D J 1996 *Appl. Opt.* **35** 1464-72
[14] Chen X, Zhu X, Li S, Ma X, Zhang J, Liu J and Chen W 2019 *Proc. SPIE (Hangzhou, China)* **11185** 111851C
[15] Takidaa Y, Nawata K and Minamide H 2020 *APL Photonics* **5** 061301
[16] Jacobsson B, Tiihonen M, Pasiskevicius V and Laurell F 2005 *Opt. Lett.* **30** 2281-83
[17] Henriksson M Doctoral thesis *Tandem optical parametric oscillators using volume Bragg grating spectral control,* 2010, 73 pages.
[18] Henriksson M, Tiihonen M, Pasiskevicius V and Laurell F 2007 *Appl. Phys. B* **88** 37–41
[19] Peng Y, Wei X, Nie Z, Luo X, Peng J, Wang Y and Shen D 2015 *Opt. Express* **23** 30827-32
[20] Kolker D B, Sherstov I V, Pustovalova R V, Kostyukova N Y, Boyko A A and Zenov K G 2017 *Quantum Elec.* **47** 14-19
[21] Erushin E, Nyushkov B, Ivanenko A, Akhmathanov A, Shur V, Boyko A, Kostyukova N and Kolker D 2021 to be published at *Laser Phys. Lett.*
[22] Boyko A A, Erushin E Y, Kostyukova N Y, Miroshnichenko I B, Kolker D B 2021 *Instrum. Exp. Tech.* **64** 254–58
[23] Belfi J, Beverini N, Bosi F, Carelli G, Di Virgilio A, Kolker D, Maccioni E, Ortolan A, Passaquieti R and Stefani F 2012 *J. Seismol.* **16** 757 – 66
[24] Sherstov I V and Kolker D B 2020 *Quantum Elec.* **50** 1063–67
[25] Nyushkov B, Kobtsev S, Antropov A, Kolker D and Pivtsov V 2019 *J. Light. Technol.* **37** 1359-63
[26] Nyushkov B, Ivanenko A, Smirnov S, Shtyrina O and Kobtsev S 2020 *Opt. Express*. **28** 14922-32
[27] Sherstov I V, Kolker D B, Boyko A A, Vasiliev V A and Pustovalova R V 2021 *Infrared Phys. Technol.* **117** 103858
[28] Vainio M and Karhu J 2017 *Opt. Express* **25** 4190-200
[29] Beverini N, Carelli G, De Michele A, Maccioni E, Nyushkov B, Sorrentino F and Moretti A 2005 *Opt. Lett.* **30** 32-34